DOI: 10.13009/EUCASS2023-854
Aerospace Europe Conference 2023 – 10TH EUCASS – 9TH CEAS

Assessment of RANS methods for low-Reynolds number compressible flows

D'Aniello Francesco Antonio⋆†*, Catalano Pietro*⋆
⋆ *Italian Aerospace Research Centre (CIRA)*
Via Maiorise, Capua, Italy, 81043
f.daniello@cira.it · p.catalano@cira.it
†Corresponding author

Abstract

The Triangular, NACA 0012-34 and Ishii airfoils have been selected for the compressible low-Reynolds aerodynamics in Martian atmosphere. All respect shape characteristics suggested in literature, delivering high aerodynamic performance in a low-Reynolds number region. The CIRA in-house developed code UZEN has been applied by employing several turbulence models to carry out the analysis on the three selected airfoils. Numerical results are globally in good agreement with experimental data in terms of aerodynamic coefficients. The complex flow field around the airfoils has been discretely reproduced. Further investigations seem to indicate that increasing Mach number does not critically affect the flow field.

1. Introduction

The present paper is related to activities developed within the CIRA-PRORA program TEDS (Favaloro *et al.*[1]), in accordance with the objectives of the PRORA program of the Italian Ministry of Research. TEDS has the main goal to develop and/or increase the TRL level of the enabling technologies for the space exploration and colonisation. One of the tasks of TEDS program concerns the evaluation of the aerodynamic characteristics of airfoils and wings in the low Martian atmosphere for the understanding of the feasibility of this type of technological solution, i.e. robotic rotorcraft to aerial survey of Martian terrain. The interest for the compressible aerodynamics of low-Reynolds number flow has recently grown for the possible use of robotic aircrafts for exploring the Martian surface. The flight in the Martian atmosphere is characterised by low Reynolds numbers (10^4 - 10^5) and by values of the Mach number in the compressible or transonic range (0.2 - 0.7). Unfortunately, the pair of compressible/transonic Mach and low Reynolds does not occurs in the low Earth's atmosphere which is characterized by the incompressible regime. For this reason, low-Reynolds number compressible flows were scarcely investigated so far, and experimental data of airfoils flying in this aerodynamics are very limited. Only NASA and JAXA agencies have experimentally studied this aerodynamic regime, as it can be noted in Fig. 1.
Therefore, an assessment of the physical/numerical models used in CFD codes must be necessary for this new flight conditions, with a particular focus on the RANS methods. The first step in achieving these objectives is a preliminary study to identify case studies of airfoils and wings configurations with experimental data obtained in "Martian" tunnels such as the Mars Wind Tunnel (MWT) that operates with low-density CO_2 at the University of Tohoku (see Munday *et al.*[4] , Anyoji *et al.*[2] , Anyoji *et al.*[5]). This because Martian atmosphere is more rarefied than Earth's one, in fact it mostly consists of carbon dioxide CO_2 (95%) and is characterized by low pressure (p $\approx$ 0.0075 $\times$101.3 kPa), low density ($\rho \approx 0.017\ kg/m^3$), and low temperature at the surface with respect to the Earth surface (as summarized in Tab. 1). The combination of low Reynolds numbers and high subsonic Mach numbers implies a flow field highly complicated with a strong interaction effect and compressibility effect. In fact, in the range of Reynolds number of 10^4 to 10^5, complicated flow phenomena including separation, transition and reattachment (see Fig. 2) take place on the wing surface and strongly affect the flight performance. Particularly, laminar separation bubbles play an important role in determining pressure distributions on the wing and aerodynamic characteristics.
The flight Mach number increases up to 0.7 since the speed of sound is low in the CO_2-based Martian atmosphere because of the low temperatures that characterizes the low Martian altitudes. The compressibility effects can play a role in suppressing the onset of shear-layer instability and the resulting formation of wake vortices, i. e. in the separation region where the formation of large-scale vortices occurs, that is a physic phenomenology typical of the

DOI: 10.13009/EUCASS2023-854

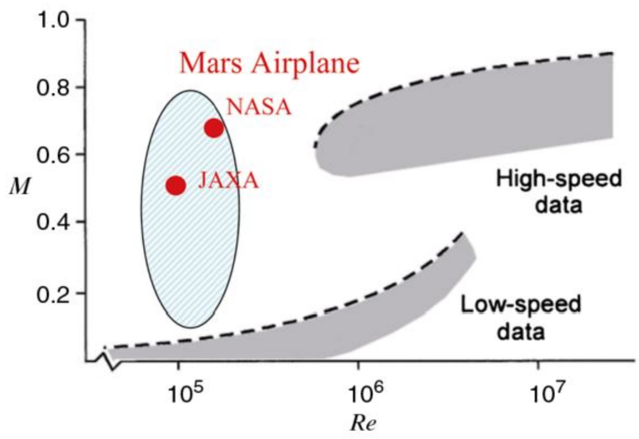

Figure 1: Martian atmospheric flight (see Anyoji *et al.*[2] and Schmitz[3])

Table 1: Comparison of environment between Mars and the Earth (from Koning *et al.*[6]).

		Mars	**Earth**
Acceleration of gravity	$[m/s^2]$	3.66	9.81
Atmospheric pressure	[kPa]	0.6÷1	101.325
Atmospheric Temperature	[K]	223.15	288.15
Atmospheric Density	$[kg/m^3]$	0.0167	1.225
Dynamic Viscosity	[kg/(ms)]	1.289×10^-5	1.789×10^-5
Gas Constant	[J/(kgK)]	192	287
Specific Heat Ratio	[-]	1.29	1.4
Speed of Sound	[m/s]	228	340

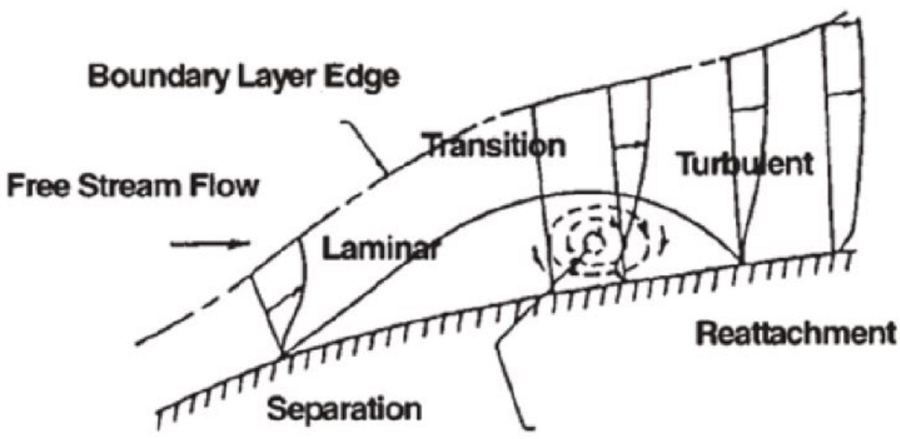

Figure 2: Flow when separation bubbles occur (see Tsukamoto *et al.*[7] and Rinoie *et al.*[8]).

incompressible low Reynolds flow. The combination of the physical phenomena described above, makes the aerodynamic performances of the airfoils and wings to behave in a unique manner. The complicated flow phenomena (separation, transition, and reattachment) that occur on the wing surface, strongly affect the aerodynamic performances of airfoils (O'Meara *et al.*[9] and Anyoji *et al.*[5]), in fact the maximum lift-to-drag ratio of airfoils significantly deteriorates because of earlier flow separation; moreover, the lift curve shows a non-linear trend, caused by the formation or burst of a laminar separation bubble, which plays an important role in determining the pressure distribution on the wing (Mueller *et al.*[10] and Anyoji *et al.*[5]). Because of these unusual flow characteristics, airfoil shape largely impacts on the aerodynamic characteristics. In fact, Schmitz (Schmitz[3,11]) has suggested three shape characteristics involving high aerodynamic performances in low-Reynolds number compressible regime:

DOI: 10.13009/EUCASS2023-854

- a sharp leading edge to fix the separation point and improve its Reynolds-number dependence on the aerodynamic performance;
- a flat upper-surface to reduce the separation region;
- a cambered airfoil to gain a lift higher than a symmetric airfoil.

The results revealed that the airfoil shape of the upper surface dominates both the formation of laminar separation bubbles and the transition to turbulence. Three suitable airfoils (in Fig. 3 sketches of the three selected airfoils, are shown) are found among the studies examined, compatible with the features required to flight in low Mars atmosphere:

- Triangular airfoil (Munday *et al.*[4])
- NACA 0012-34 (Anyoji *et al.*[2])
- Ishii airfoil (Anyoji *et al.*[5])

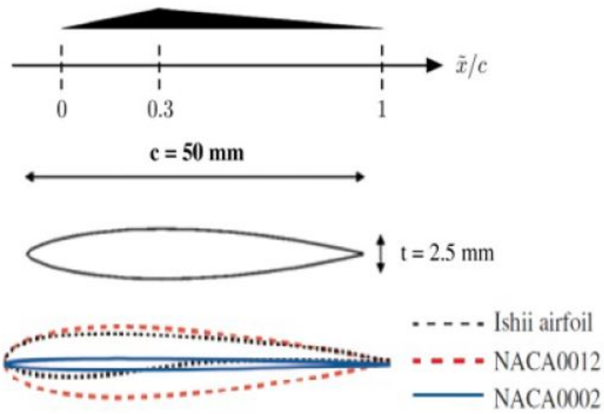

Figure 3: Triangular (top), NACA0012-34 (centre) and Ishii airfoils (bottom).

2. Numerical method

The numerical analysis is conducted by using the CIRA in-house developed flow solver UZEN. The code (Catalano *et al.*[12]) solves the compressible 3D steady and unsteady RANS equations on block-structured meshes. The spatial discretization adopted is a central finite volume formulation with explicit blended 2^{nd} and 4^{th} order artificial dissipation. The dual-time stepping technique is employed for time accurate simulations (Marongiu *et al.*[13] , Vitagliano *et al.*[14]). The pseudo-time integration is carried out by an explicit hybrid multistage Runge-Kutta scheme. Classical convergence acceleration techniques, such as local time stepping and implicit residual smoothing, are available together with multigrid algorithms. Turbulence is modelled by either algebraic or transport equation models (Catalano *et al.*[15]). Structured multi-block grids were built by using ICEM CFD© commercial code for all the selected airfoils. The level of grid mesh and the number of cells for each level for the three considered airfoils are listed in Tab. 2. Both RANS and URANS numerical simulations were conducted to reproduce the MWT experimental data collected in the selected bibliography for all the three airfoils. Focus is placed in the aerodynamic performance coefficients, i.e. lift (C_L) and drag coefficient (C_D) to better understand how the aerodynamic performance change in the Mars atmosphere respect to the Earth one.

3. Triangular airfoil

The experiment in the MWT (see Fig. 4), that is the low density CO_2 test facility of Tohoku University (Nose *et al.*[16] and Anyoji *et al.*[2]) over a Triangular airfoil with global forces and local PSP measurements, has been considered to first assess the UZEN code.
A structured multi-block grid resembling the airfoil placed in the wind tunnel has been kindly provided by ONERA (Fig. 5). The number of blocks is 33 and the number of cells is about 14×10^6. Three meshes with the airfoil set in the

DOI: 10.13009/EUCASS2023-854

Table 2: Grid levels and number of cells (ni x nj x nk; nk=1) for the Triangular airfoil, NACA 0012-34 and Ishii airfoil.

	$1^{st}lev$	$2^{nd}lev$	$3^{rd}lev$	$4^{th}lev$
Triangular	2×10^6	15×10^6	/	/
	(nk=64)	(nk=130)		
NACA 12-34	200×25	400×50	800×100	1600×200
	5000	20000	80000	320000
Ishii	64×32	128×64	256×128	512×256
	2048	8192	32768	131072

Figure 4: Mars Wind Tunnel (MWT) of the Tohoku University.

wind tunnel at $\alpha = 5°$, 10°, and 15° have been made available. The grids allow for the resolution of the boundary layer on all the tunnel walls (Fig.5). Numerical simulations have been performed at $\alpha = 5°$, 10°, and 15°, Mach number 0.15, 0.50, and 0.70, and Reynolds number 3.0×10^3, and 1.0×10^4.

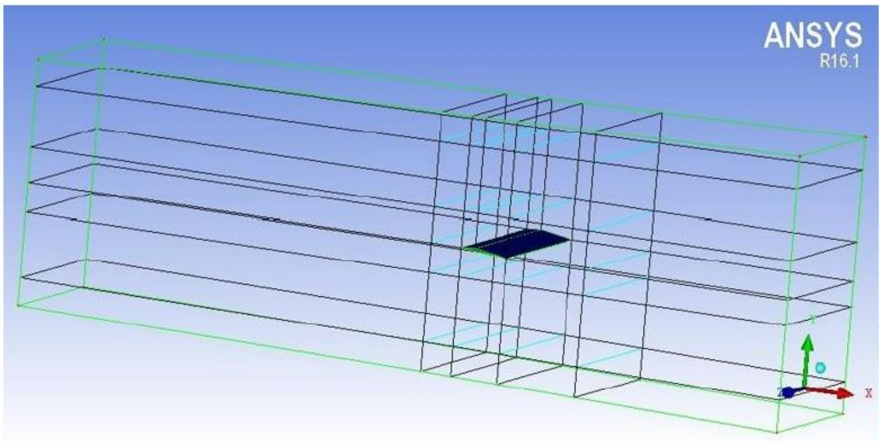

Figure 5: Triangular airfoil in Tohoku wind tunnel. Topology of the grid.

3.1 Preliminary numerical results at $\alpha = 5°$

The pressure coefficient at the mid-span section of the airfoil achieved at Mach=0.50, and Reynolds number=3.0×10^3 is compared to the experimental data in Fig. 6. A laminar flow and a turbulent flow by four turbulence models, the $\kappa - \omega$ TNT, SST, SST-LR[17] and SST-γ, have been considered.

DOI: 10.13009/EUCASS2023-854

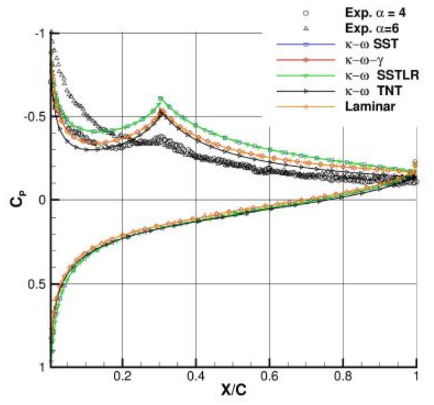

Figure 6: Pressure coefficient at α = 5°, Mach=0.50, and Reynolds number=3.0×10^3.

Experimental c_p [1] are available at α = 4° and 6°. The agreement is not very good with an over-prediction on the rear region of the upper surface. The c_p returned by the $\kappa - \omega - \gamma$ model is very similar to the laminar solution, as expected considering the value of the Reynolds number. The $\kappa - \omega$ SST and SST-LR provide the same result with difference to the $\kappa - \omega$ TNT. This could be explained by considering that the boundary layer of the WT walls has been taken into account only by the $\kappa - \omega$ TNT model. The effect of the Mach number is shown in Fig. 7 at Reynolds numbers 1.0×10^3, for instance through $\kappa - \omega$ TNT turbulence model. The effect is more remarkable on the upper surface and is the same at both Reynolds numbers. The flow expands more in the front part and less in the rear part of the airfoil as the Mach number decreases.

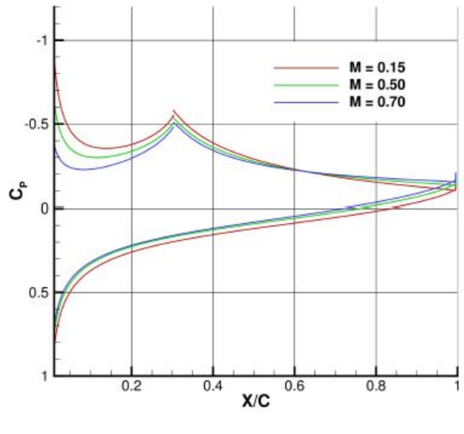

Figure 7: Pressure coefficient at α = 5°. Effect of Mach number at Reynolds number 1.0×10^3, through $\kappa - \omega$ TNT.

The effect of the Reynolds number is shown in Fig. 8 at the three Mach numbers investigated. The Reynolds number has an influence on the pressure levels on the upper surface of the airfoil. The flow tends to have a greater expansion peak as the Reynolds number increases. This effect is returned clearly by the $\kappa - \omega$ TNT model. It is evident in all the plots that the compression downstream the leading-edge expansion becomes stronger at the highest Reynolds number. A stronger compression occurs in the rear zone as the Reynolds number increases.

3.2 Preliminary numerical results at α = 10°

At this incidence, some turbulence models have shown poor convergence, and time-accurate simulations should have been necessary. The pressure coefficient at Mach=0.50, and Reynolds number equal to 3.0×10^3 is presented in Fig. 9. The comparison with the experimental data is not good. The flow is separated in the experiments on a large portion of the airfoil, while the $\kappa - \omega$ TNT and SST provide an attached flow at the mid-span section of the model.

[1] All experimental data for Triangular airfoil are available in Munday *et al.*[4]

DOI: 10.13009/EUCASS2023-854

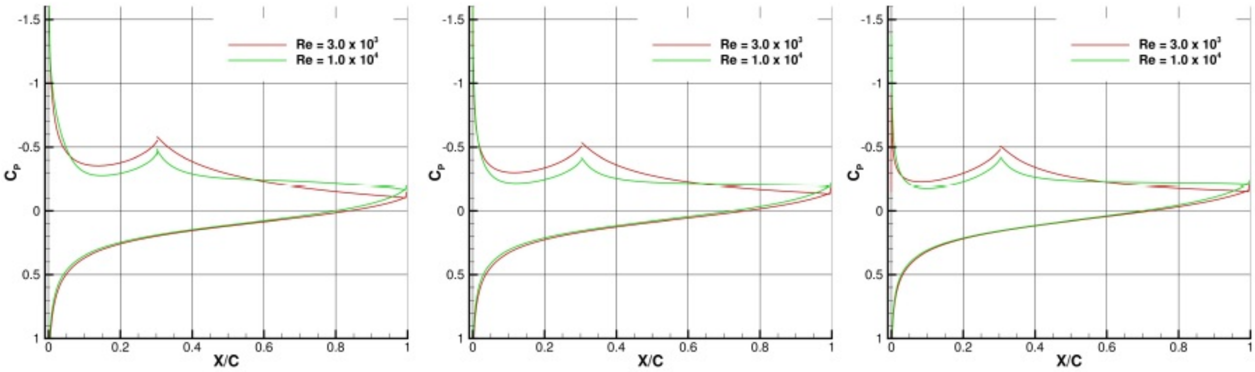

(a) M = 0.15 (b) M = 0.50 (c) M = 0.70

Figure 8: Pressure coefficient at $\alpha = 5°$, at Mach = 0.15, 0.5, 0.7, through $\kappa - \omega$ TNT turbulence model. Effect of Reynolds number.

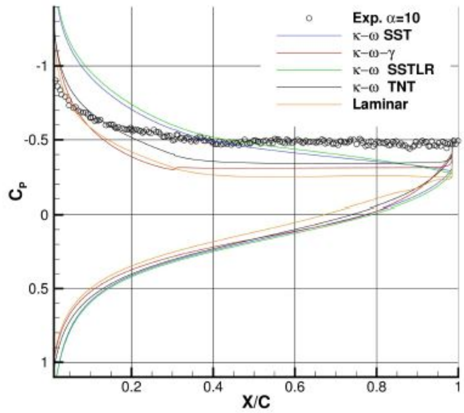

Figure 9: Pressure coefficient at $\alpha = 10°$, Mach=0.50, and Reynolds number = 3.0×10^3.

This is confirmed in Fig. 10 that shows the pressure distribution and the skin friction lines on the upper surface of the airfoil. The flow is fully attached in the central region of the model while some 3D effects can be noted at the side-ends of the model.

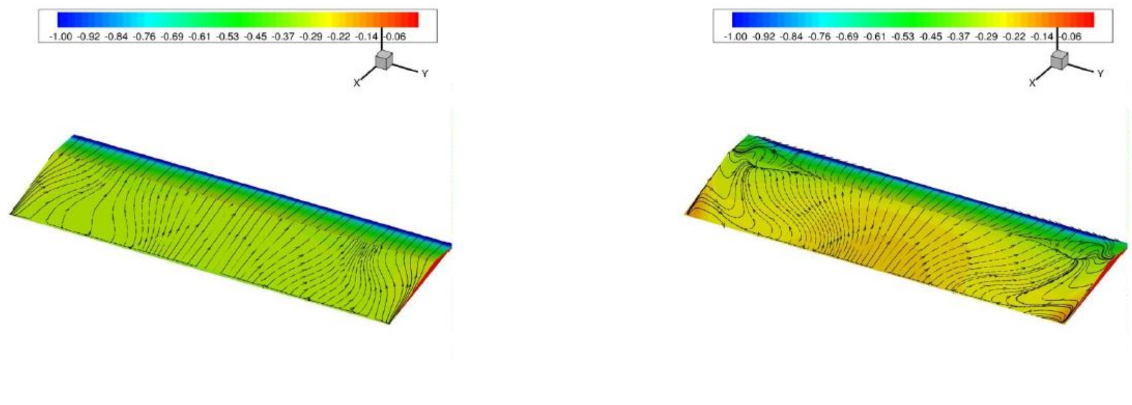

(a) Re = 3.0×10^3 (b) Re = 1.0×10^4

Figure 10: Pressure coefficient and skin friction lines on the upper surface of the airfoil at M = 0.50, Re = 3.0×10^3 and at $\alpha = 10°$.

DOI: 10.13009/EUCASS2023-854

Therefore, the effect of Mach and Reynolds number has been investigated by this model. The effect of the Mach number is shown in Fig. 11 and is similar to the one observed at $\alpha = 5°$. The expansion in the front part and the compression in the rear region increase with the Mach number.

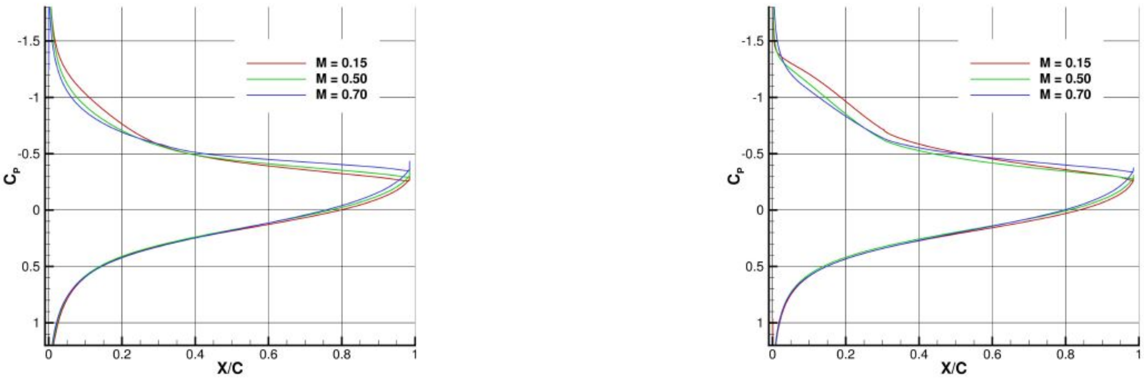

(a) Re = 3.0×10^3 (b) Re = 1.0×10^4

Figure 11: Pressure coefficient at $\alpha = 10°$. Effect of Mach number by the $\kappa - \omega$ SST turbulence model.

The effect of the Reynolds number is presented in Fig. 12. The flow tends to expands more as the Reynolds number increases. This is much more evident in the front part and becomes almost negligible in the rear region of the airfoil.

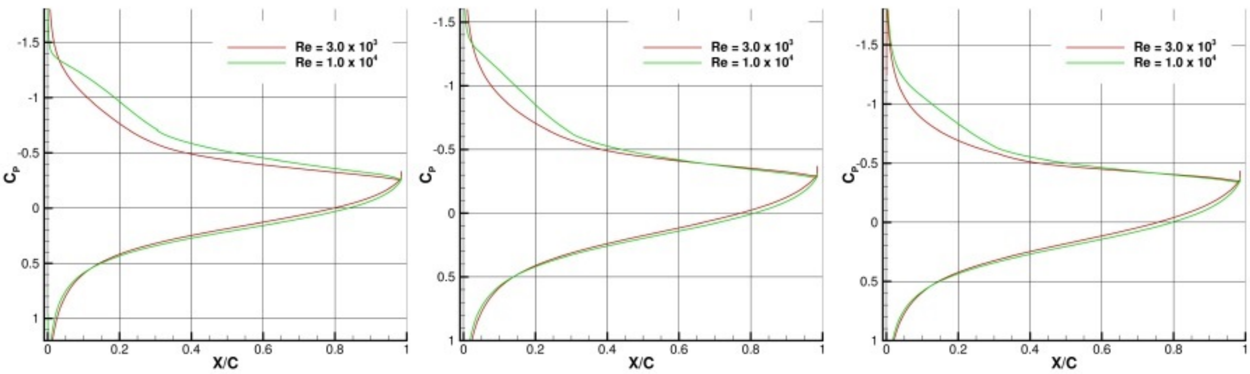

(a) Mach = 0.15 (b) Mach = 0.5 (c) Mach = 0.7

Figure 12: Pressure coefficient at $\alpha = 10°$. Effect of Reynolds number by the $\kappa - \omega$ SST model.

3.3 Preliminary numerical results at $\alpha = 15°$

Time-accurate simulations have been needed at this incidence. This has been necessary at the lowest Mach and Reynolds numbers. A reasonable convergence, instead, has been obtained at the highest Mach numbers and Reynolds of 1.0×10^4 by steady RANS computations.

The flow field provided by the numerical simulations is quite complex. Fig. 13 reports the flow field in terms of surface pressure distribution and skin friction lines as provided by the $\kappa - \omega$ TNT turbulence model. Side-ends effects and separation regions in the central part of the model downstream the vertex of the triangle are visible at all the flow conditions. The trace of a horseshoe-shaped vortex can be discerned at M=0.50 and Re=3.0×10^3.

The flow structures forming at the side-ends of the body and developing in the wake can be also appreciated in Fig. 14 that reports an iso-surface of $Q = \frac{1}{2}\left(\Omega_{i,j}\Omega_{i,j} - S_{i,j}S_{i,j}\right)$. The vortex regions in the central part are visible. It can be also observed as the side-end structures tend to disappear at the highest Reynolds number.

The time-averaged pressure coefficient achieved by the $\kappa - \omega$ TNT turbulence model is compared to the experimental data in Fig. 15. A fully separated flow on the upper surface is returned by both experiments and numerical simulations. The level of c_p is overestimated. The effect of the Mach number is shown in Fig. 16. The flow is separated at all the

DOI: 10.13009/EUCASS2023-854

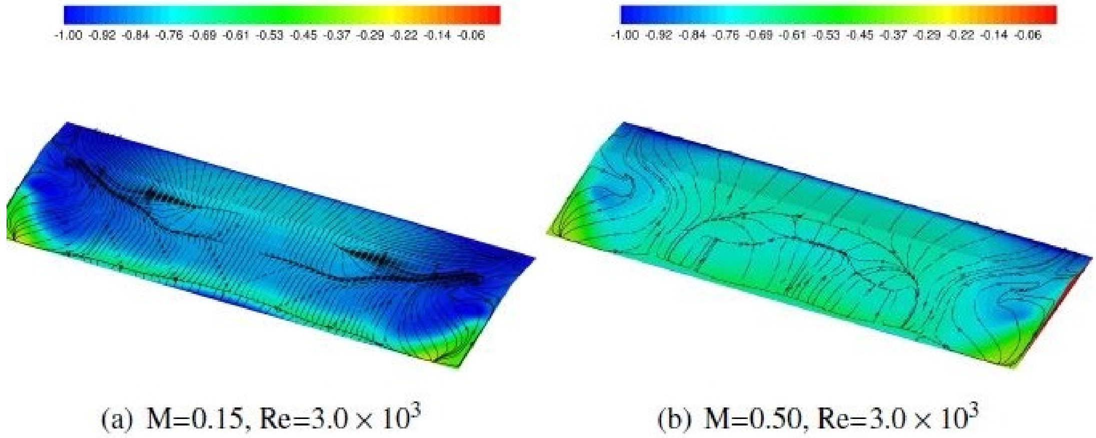

Figure 13: Pressure distribution and skin friction lines at α = 15°.

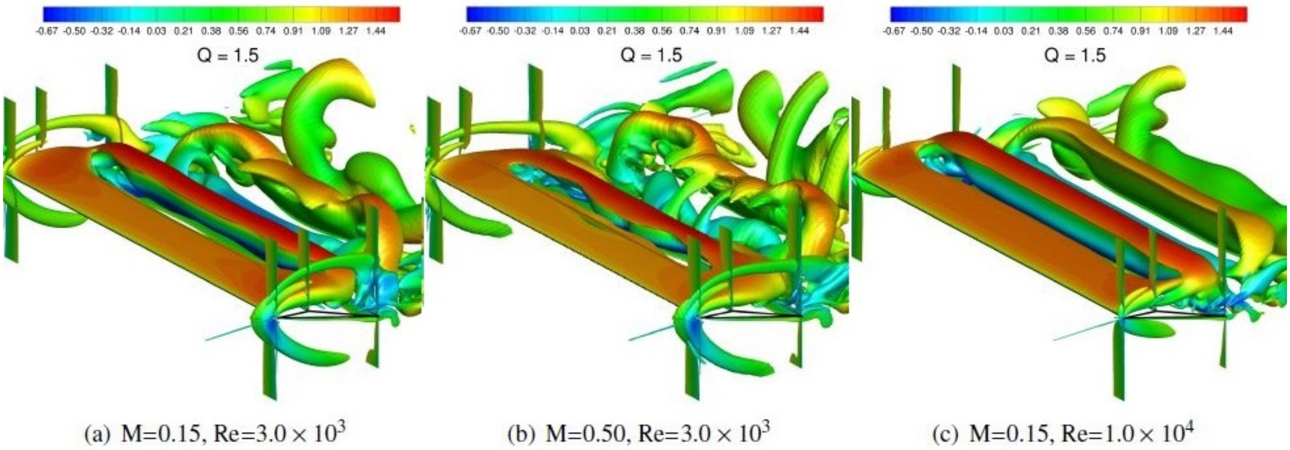

Figure 14: Isosurface of Q at α = 15°.

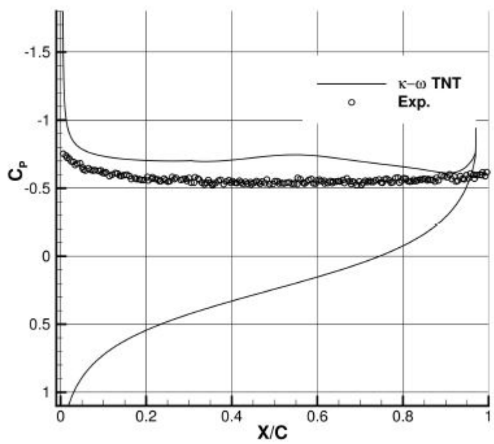

Figure 15: Pressure coefficient at Mach 0.50, Re=3.0×10^3, and α = 15°.

Mach numbers but the levels of pressure on the upper surface become lower as the Mach increases.The effect is more evident between Mach 0.15 and Mach 0.50. At Mach number 0.70, the effect of a vortex seems to be present in the rear region of the airfoil.

DOI: 10.13009/EUCASS2023-854

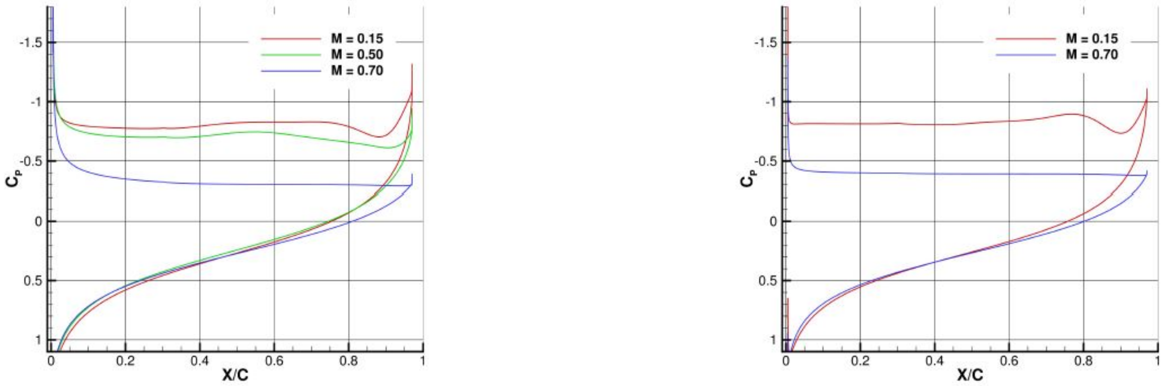

(a) Re = 3.0×10^3

(b) Re = 1.0×10^4

Figure 16: Pressure coefficient at $\alpha = 15°$. Effect of Mach number by the $\kappa - \omega$ TNT turbulence model.

3.4 Aerodynamic coefficients

The lift curves and the drag polars are shown in figures 17 and 18 for Reynolds number 3.0×10^3 and 1.0×10^4 respectively. Only the numerical results achieved by simulations with a good level of convergence are reported in the plots. At Reynolds number 3.0×10^3, all the numerical models have provided lift coefficients in good agreement with the experiments at $\alpha = 5°$ for all the three Mach numbers considered. As the incidence increases, the comparison gets worse as expected. At $\alpha = 10°$, only the lift coefficient returned by the $\kappa - \omega$ SSTLR is acceptable, while a large discrepancy is obtained at $\alpha = 15°$. The $\kappa - \omega$ SST provides a C_L in very good agreement with the experiments at Mach 0.70 and $\alpha = 15°$. The analysis of the drag polars is very interesting. The agreement between numerical and experimental data is quite good except for Mach 0.15 at the high values of the lift coefficient. The behaviour and the trend of the polars is well reproduced at all the Mach numbers. At Reynolds number 1.0×10^4, laminar simulations have not been performed because the hypothesis of laminar flow has been assumed only at Reynolds number 3.0×10^3. The agreement with the experimental data is better than at Re = 3.0×10^3. The comparison for the lift coefficient is more than acceptable at all the incidences and Mach numbers with some more discrepancy at Mach 0.70. The non linearity and the behaviour of the C_L curves seems to be captured by the numerical simulations. A good comparison with the experiments is shown for the drag polars. At M = 0.15, the agreement is very good, while some discrepancy can be noted at Mach 0.50 and 0.70 at the high values of C_L and C_D. However, behaviour and trend of the curves are well reproduced at all the Mach numbers.

4. NACA 0012-34

NACA 0012-34 is a more feasible flying airfoil than the Triangular one, because its flat symmetric shape allows to show the effect of the viscosity on the aerodynamic performances, and its small leading-edge radius allows to border an early laminar separation in the vicinity of the leading edge itself. Lift curve and polar curve[2] have been reproduced for NACA 0012-34 airfoil, through both RANS and URANS numerical simulations. Particularly, time-accurate simulations have been needed at $\alpha = 0°$ and 1° because the formation of vortex shedding in the wake. A reasonable convergence has been obtained at the lower and intermediate incidences and lower Mach numbers by steady RANS computations. URANS have been necessary at the higher angles of attack at the highest Mach number. Reynolds number is set at 1.1×10^4 according to experimental tests and data reported in Anyoji *et al.*[2] The specific heat ratio γ is set equal to 1.3 which is the value that characterizes the low Martian atmosphere rich of CO_2. Steady simulations and time-accurate simulations have been performed by different $\kappa - \omega$ models: SST, TNT, SSTG (i. e. SST-γ). Lift curves and drag polars for the three considered Mach numbers are shown in figures 19 and 20, respectively.
As it can be seen in these figures, numerical results are in good agreement in terms of C_L at $\alpha = 0°$ and $\alpha = 1°$ for all the used turbulence models. An underestimation of the C_L is shown for all the used turbulence models and at all the considered Mach numbers in the range of $\alpha = 2° - 7°$. The difference between the numerical curves and the experimental ones becomes wider as α increases. At higher Mach numbers and in the same range of α a better agreement with experimental data is reached, especially for the $\kappa - \omega$ SST that allows to reproduce the correct linearity

[2]All experimental data for NACA 0012-34 airfoil are reported in Anyoji *et al.*[2]

DOI: 10.13009/EUCASS2023-854

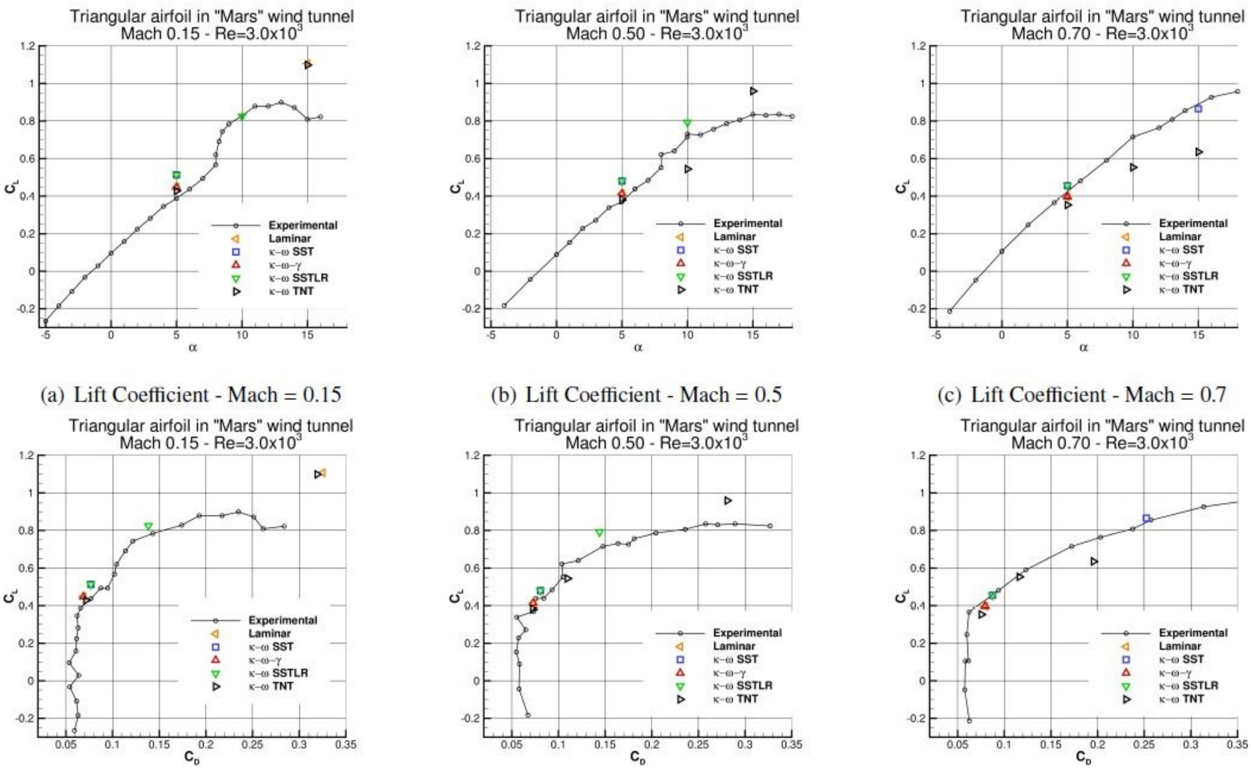

(a) Lift Coefficient - Mach = 0.15 (b) Lift Coefficient - Mach = 0.5 (c) Lift Coefficient - Mach = 0.7

(d) Drag Polar - Mach = 0.15 (e) Drag Polar - Mach = 0.5 (f) Drag Polar - Mach = 0.7

Figure 17: Lift coefficients and drag polars at Reynolds number 1.0×10^3.

of the lift curve. Moreover, in terms of C_D it can be noted a slight underestimation for all the considered Mach numbers. At the highest Mach numbers, especially at Mach equal to 0.61, the drag polars are closer to the experimental values. This because the Mach number increasing introduces compressibility effect that may allow to reduce the vortex shedding in the wake, especially at high incidences ($\alpha = 2° - 6°$). The reported underestimation both in terms of C_L and C_D is due to the used turbulence models that are not be able to reproduce exactly the very complex flow field (vortex structure, laminar separation bubble, etc) generated around the wing. It could be said that the global linear part of the lift curves is reproduced with a slight underestimation, while the non-linear part is not reproduced because of the lack of convergence of the numerical simulations. The flow field at high incidences is more complex than at the low incidences, thus generating the non-linear behaviour of the aerodynamic performances curves.

In Fig. 21 the pressure coefficient on the upper surface of the airfoil at $\alpha = 0°, 7°$, Re $= 1.1 \times 10^4$ and M = 0.20 calculated with different $\kappa - \omega$ turbulence models is compared to experimental data. It can be noted a slight underestimation at $\alpha = 7°$ that confirms the lower value for C_L, as previously underlined, for the lift curve.

In Fig. 22, Mach contours with streamlines at $\alpha = 7°$, Re $= 1.1 \times 10^4$ at the three different Mach numbers calculated with $\kappa - \omega$ SST turbulence models, are reported. Contours underline that the expansion peak is bound in the proximity of the leading edge of the airfoil, at high incidences, thanks to the sharp shape of the leading edge itself. Separated flow accompanied by vortex shedding, invests almost the entire upper surface of the airfoil, forming an intense shear layer. The increase in Mach numbers does not critically influence the flow field. It seems, on the contrary, that Mach number energizes the flow, making weaker the shedding of smaller vortexes from the stronger one, that forms already at $\alpha = 4°$ and becomes stronger as α increases. Therefore, higher Mach numbers are more able to withstand with the adverse pressure gradients, making the flow becomes less prone to the separation.

In figures 23 and 24 are reported the pressure coefficient on the body at Re $= 1.1 \times 10^4$, calculated through different $\kappa - \omega$ models at $\alpha = 0°, 3°, 5°, 7°$, at M = 0.48 and M = 0.61, respectively. A good comparison between different turbulence models is shown in terms of pressure coefficient [3].

[3]Post-processed experimental data for NACA 0012-34 airfoil are not available in Anyoji *et al.*[2] at Mach equal to 0.48 and 0.61.

DOI: 10.13009/EUCASS2023-854

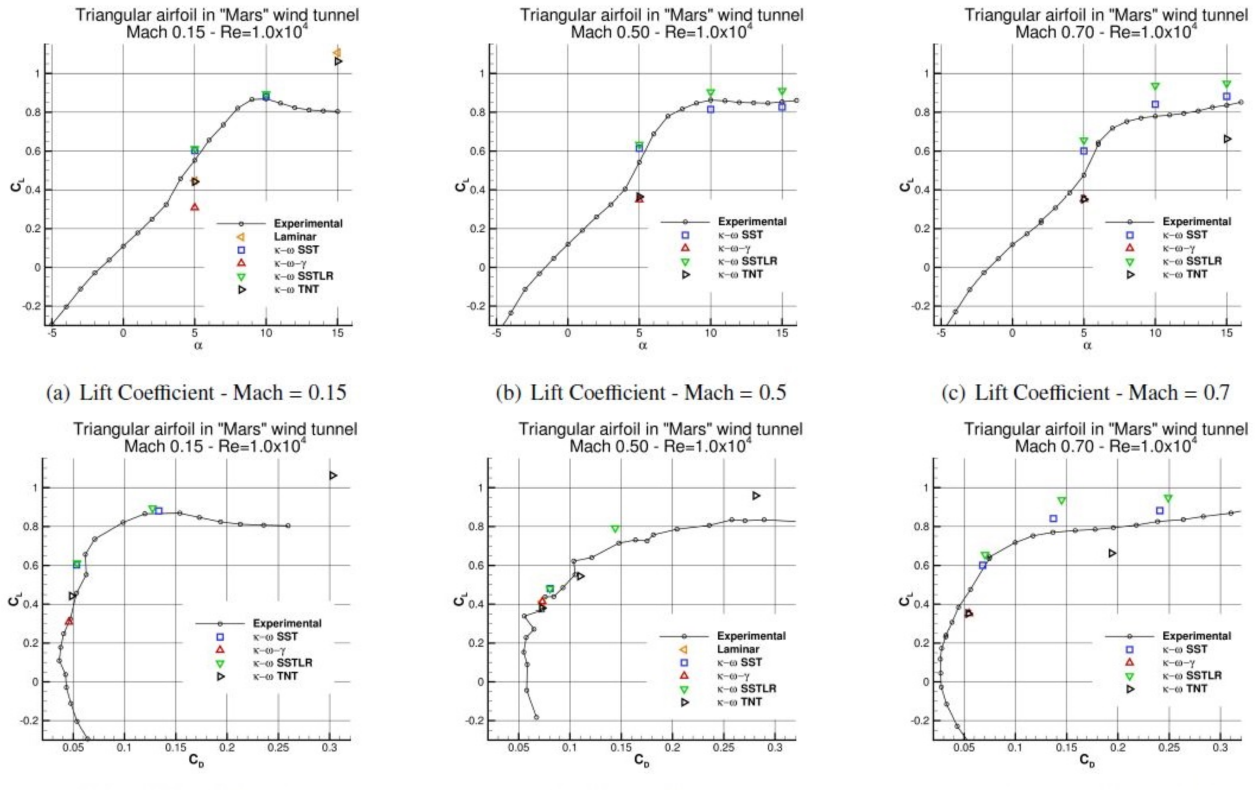

(a) Lift Coefficient - Mach = 0.15 (b) Lift Coefficient - Mach = 0.5 (c) Lift Coefficient - Mach = 0.7

(d) Drag Polar - Mach = 0.15 (e) Drag Polar - Mach = 0.5 (f) Drag Polar - Mach = 0.7

Figure 18: Lift coefficients and drag polars at Reynolds number 1.0×10^4.

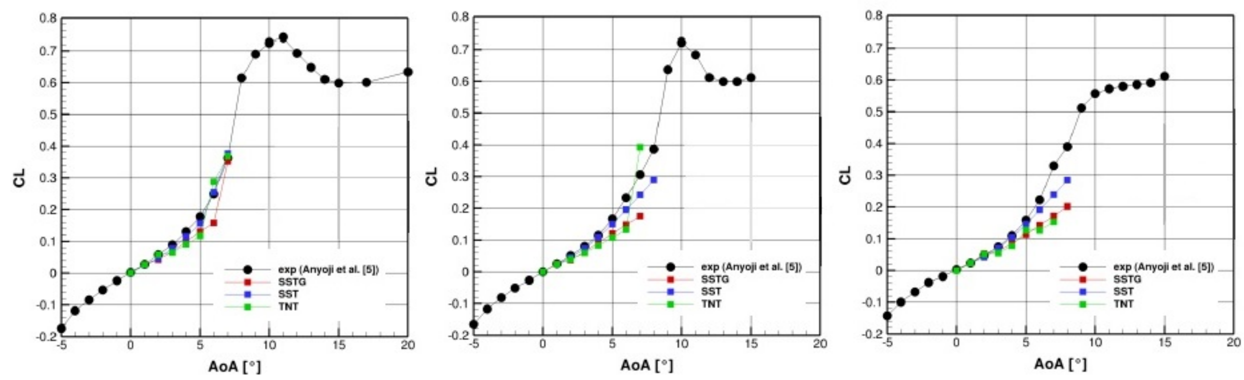

(a) Mach = 0.20 (b) Mach = 0.48 (c) Mach = 0.61

Figure 19: Lift coefficient curves at Re = 1.1×10^4, at M = 0.20, 0.48, 0.61, calculated with different $\kappa - \omega$ turbulence models.

5. Ishii airfoil

Ishii airfoil has all the features listed by Schmitz[3] . Therefore, it is considered a more feasible flying airfoil than Triangular and NACA 0012-34 ones. Moreover it is confirmed in Nose *et al.*[18] and in Anyoji *et al.*[19] that Ishii airfoil has weak Reynolds number dependence in the range from Re = 2.3×10^4 to Re = 4.6×10^4. The laminar separation bubble plays an important role in determining the pressure distribution on the wing and the aerodynamic characteristics in the low-Reynolds compressible regime causing a non-linear lift curve (Anyoji *et al.*[5]). This can be seen in Fig. 25 where the numerical data obtained from the current study are compared with the experimental data and numerical simulations (LES) data collected by Anyoji *et al.*[5] for Ishii airfoil. The aerodynamic performances, i.e. lift coefficient

DOI: 10.13009/EUCASS2023-854

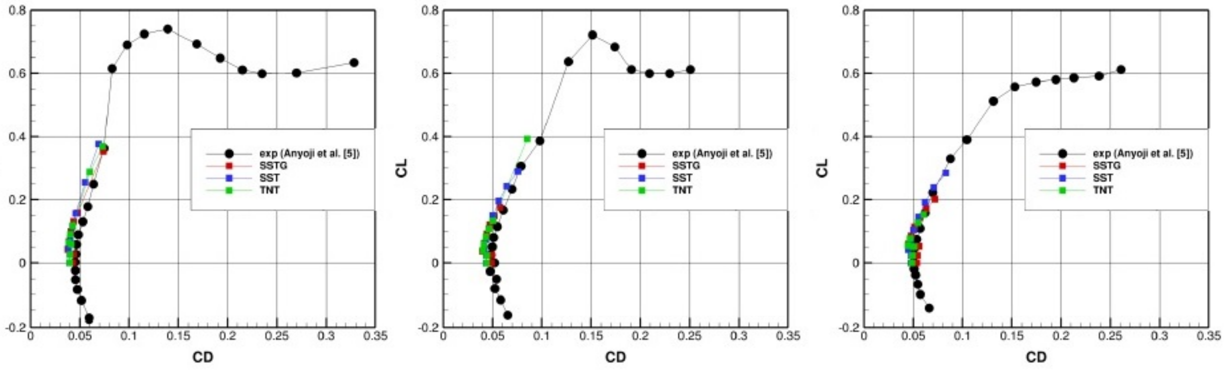

(a) Mach = 0.20 (b) Mach = 0.48 (c) Mach = 0.61

Figure 20: Drag Polars at Re = 1.1×10^4, at M = 0.20, 0.48, 0.61, calculated with different $\kappa - \omega$ turbulence models.

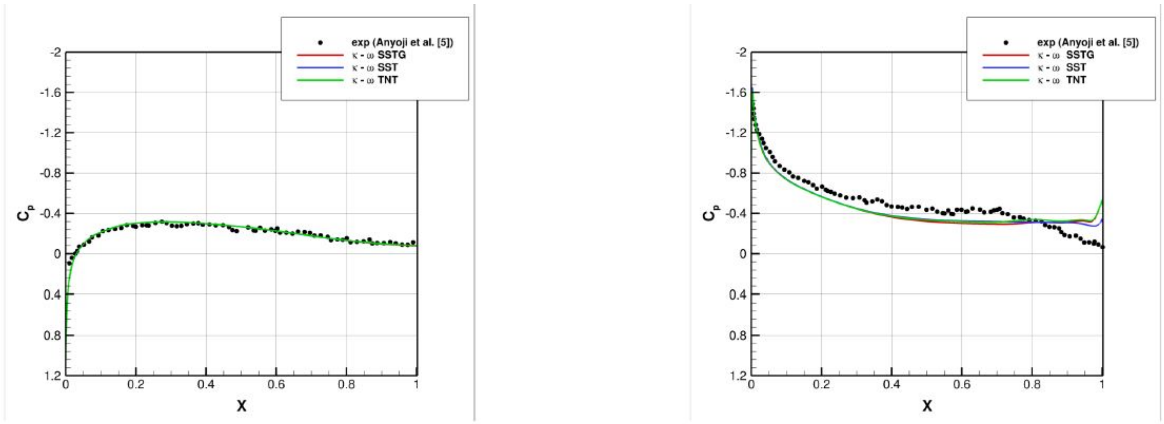

(a) $\alpha = 0°$ (b) $\alpha = 7°$

Figure 21: Pressure coefficient at $\alpha = 0°, 7°$, Re = 1.1×10^4 and M = 0.20 calculated with different $\kappa - \omega$ turbulence models.

(a) M = 0.20

(b) M = 0.48

(c) M = 0.61

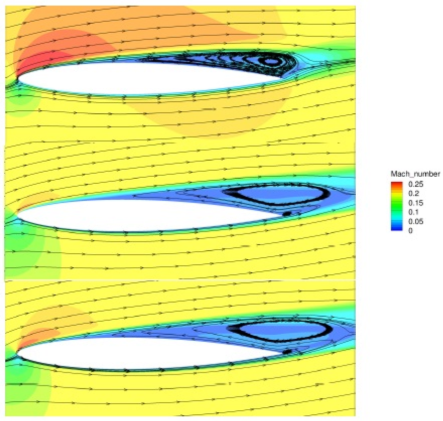

Figure 22: Mach contours at $\alpha = 7°$, Re = 1.1×10^4 calculated with $\kappa - \omega$ SST, at three different Mach numbers.

C_L and drag coefficient C_D, have been calculated at Mach = 0.20, Re = 2.3×10^4 and $\gamma = 1.3$.
In Fig. 25 both C_L and C_D curves are partially reproduced due to the lack of numerical convergence. Fig. 25 shows that all the $\kappa - \omega$ turbulence models gave a slight overestimation in terms of C_L and a slight underestimation in terms of C_D with respect to the experimental data. The $\kappa - \omega$ turbulence models used and the mesh used for Ishii airfoil does not

DOI: 10.13009/EUCASS2023-854

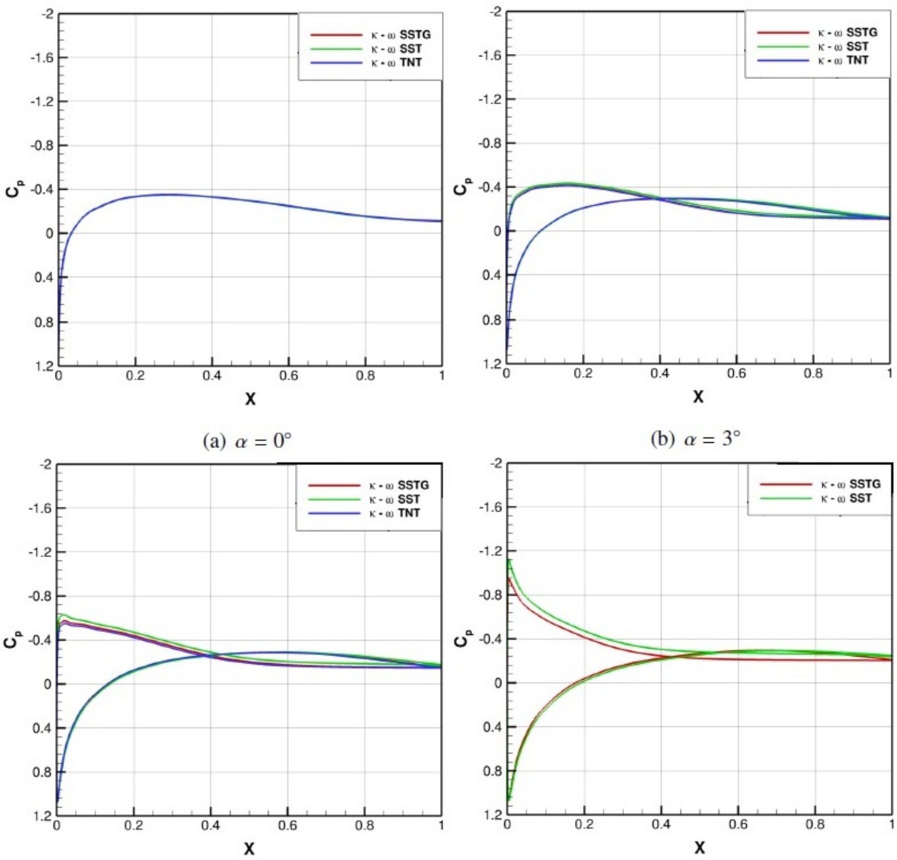

(a) $\alpha = 0°$ (b) $\alpha = 3°$

(c) $\alpha = 5°$ (d) $\alpha = 7°$

Figure 23: Pressure coefficient at Re = 1.1×10^4 and Mach = 0.48 calculated for different $\kappa - \omega$ models at $\alpha = 0°, 3°, 5°, 7°$.

allow to reproduce perfectly the complex flow structure that occurs on this airfoil at all the considered incidences. This is composed by laminar separation bubble plus laminar-to-turbulent transition and vortex shedding in the wake, this especially as the angle of attack increases. The $\kappa - \omega$ SST model gave a good agreement for almost all the considered incidences, especially respect to the LES numerical simulations, particularly as regards the values of C_D (Fig. 25 right). In Fig. 26, pressure coefficient c_p at $\alpha = 3°$ and 6° is shown. In this figure, it could be seen that at $\alpha = 3°$ all the $\kappa - \omega$ models, used in the simulations, converge and the results are globally in good agreement with experimental and LES data. The SSTG model gives results very similar to the LES ones. The SST and TNT models have a slight overestimation in the peak of suction. All the $\kappa - \omega$ models are slightly underestimated in the rear part of the upper surface of the wing. At $\alpha = 6°$, only the $\kappa - \omega$ SST converges. The results are slightly overestimated with respect to the literature data. in the right picture of Fig. 26, it can be seen the comparison among three different angles of attack (5°,6°,7°). It can be observed a plateau in the experimental c_p diagram, which could indicate the presence of the laminar separation bubble that forms on the upper surface of the wing. This trend is also reproduced by convergent numerical simulation, however the zone at constant c_p is smaller than the one experimentally measured. Therefore, the calculated bubble may be shorter than the one experimentally reported. The c_p at $\alpha = 7°$ is closer, than that at $\alpha = 5°$, to the experimental and LES one, especially in the peak of expansion and in the initial part of the constant trend, even though it is shorter than the one reported in the experimental data. In Fig. 27 Mach number contour with streamlines is shown, for Ishii airfoil at $\alpha = 6°$, Mach = 0.2, Re = 2.3×10^4, by the $\kappa - \omega$ SST turbulence model. Sharp leading edge, characterized by a small local curvature radius, allows to concentrate the expansion peak near the leading edge itself, at high incidences. Moreover, it can be noted a zone of recirculation of the flow (as the streamlines circles) in correspondence of the expansion on the upper surface of the airfoil, immediately downstream the leading edge. This could indicate the presence of the laminar separation bubble, as also mentioned above.

DOI: 10.13009/EUCASS2023-854

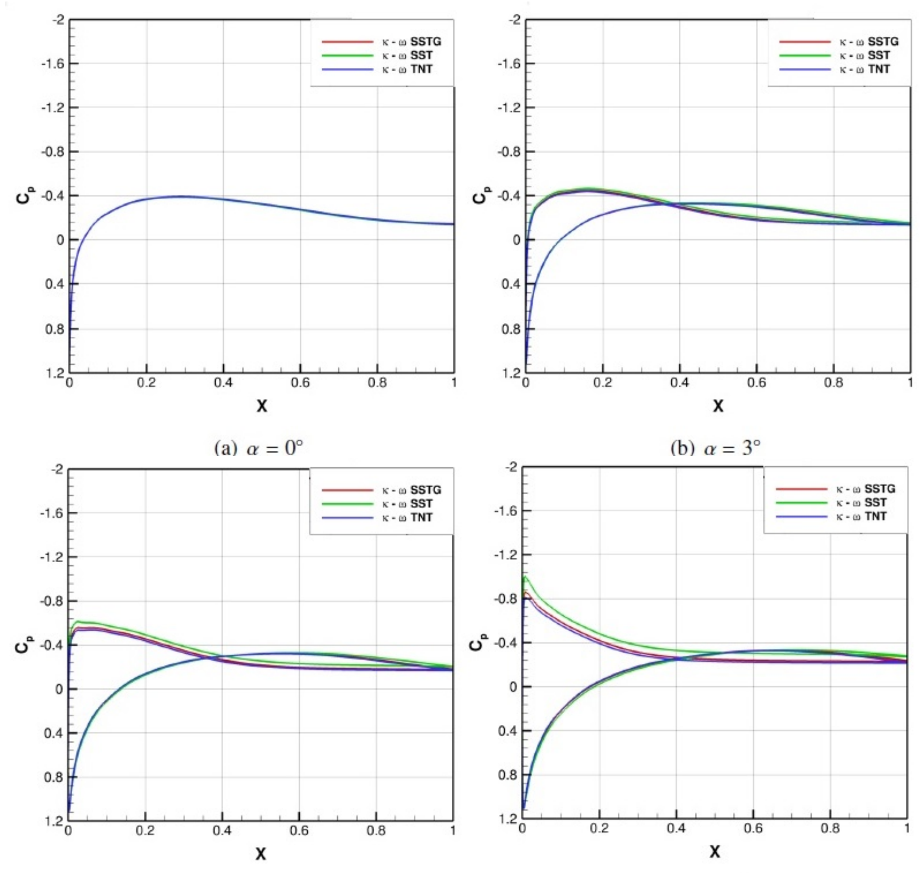

(a) $\alpha = 0°$ (b) $\alpha = 3°$ (c) $\alpha = 5°$ (d) $\alpha = 7°$

Figure 24: Pressure coefficient at Re = 1.1×10^4 and Mach = 0.61 calculated for different $\kappa - \omega$ models at $\alpha = 0°, 3°, 5°, 7°$.

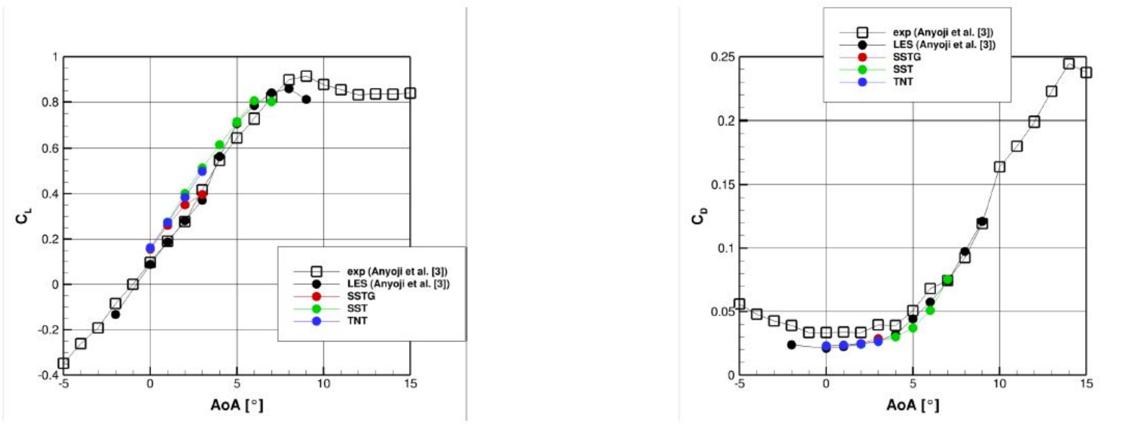

(a) Lift Coefficient (b) Drag Coefficient

Figure 25: Lift and Drag Coefficients at Reynolds number 2.3×10^4 and at Mach number 0.20, with different $\kappa - \omega$ turbulence models.

6. Conclusions

The compressible low Reynolds regime that characterizes low Martian atmosphere has been reproduced by numerical simulations performed by the CIRA in-house UZEN code. The results have been compared with experimental data reported in literature. The numerical simulations have partially reproduced the flow field around the airfoils (NACA0012-34, Ishii) and the wing (Triangular airfoil) with a globally good agreement with the experimental data

DOI: 10.13009/EUCASS2023-854

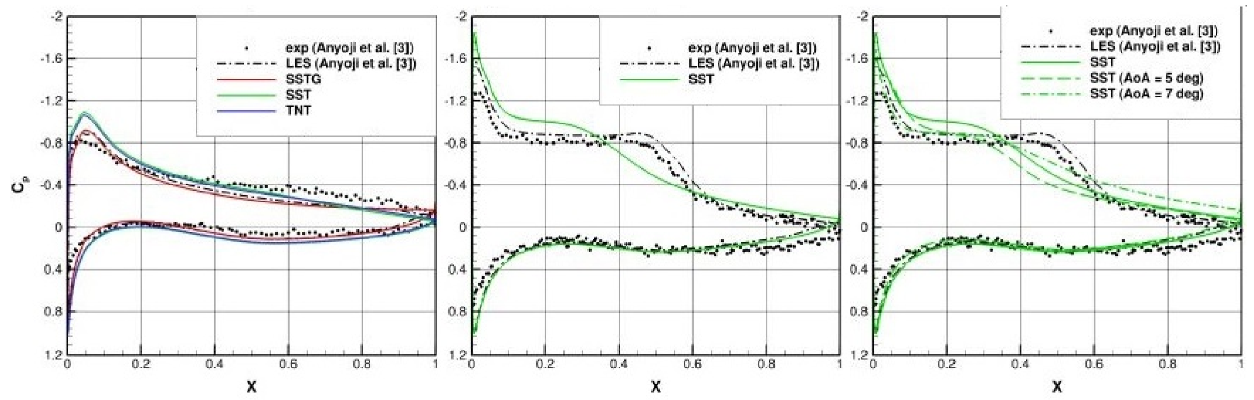

(a) $\alpha = 3°$ (b) $\alpha = 6°$ (c) Various α for $\kappa - \omega$ SST model

Figure 26: Pressure coefficient at M = 0.20, Re = 2.3×10^4 at $\alpha = 3°$ (left) and 6° (centre) for different $\kappa - \omega$ models and at different α for $\kappa - \omega$ SST model (right).

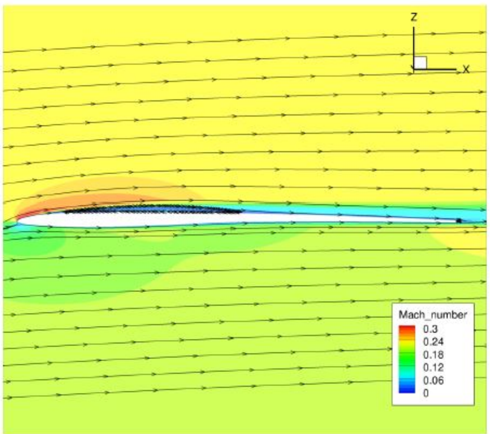

Figure 27: Mach number contour at Mach = 0.2, Re = 2.3×10^4, by the $\kappa - \omega$ SST turbulence model, at $\alpha = 6°$.

but with a globally underestimation in terms of aerodynamic performances (lift and drag coefficients). The flow over the Triangular airfoil has been simulated inside the wind tunnel. The flow field and the aerodynamic coefficients have been reasonably well reproduced at the low-medium incidences. The agreement with the entire set of the experimental data is acceptable except at the highest α where the flow is completely separated over the airfoil. However, the 3D simulations conducted on the wing based on the Triangular airfoil, have allowed to underline the strongly 3D structure of the flow field that influences the aerodynamic performance degradation, mainly at high incidences. NACA 0012-34 and Ishii are more realistic as flying airfoils than the Triangular one. Their design has been thought to fly at high incidences in a low-Reynolds environment and, at the same time, to allow the flow to reattach downstream the formation of the laminar separation bubble. Both the airfoils have been investigated almost exclusively in a two-dimensional way. The analysis on the NACA 0012-34 has partially reproduced the non-linear behaviour of the lift curves at all the Mach numbers considered and with all the $\kappa - \omega$ turbulence models used in the simulations. The employed $\kappa - \omega$ turbulence models have been capable to reproduce the complex flow field around the airfoil. Ishii airfoil respects all the geometric and aerodynamic features prescribed in literature. The same considerations drawn about the NACA 0012-34 could be repeated for the Ishii. Results of the numerical simulations are globally in good agreement with experimental data in terms of aerodynamic performances. The complex flow field has been discretely reproduced, particularly the laminar separation bubble which starts from the leading edge at $\alpha = 6°$ and then extends over almost the entire upper side of the airfoil, as the incidence increases. The numerical simulations performed on the three considered airfoils have provided results in good agreement with the experimental data, in terms of aerodynamic performances, especially at low and medium incidences. The influence of the Mach number has been also investigated. The numerical results have shown that the increase in Mach numbers does not critically influence the flow field. It seems, on the contrary, that Mach number energizes the flow that is more able to withstand with the adverse pressure gradients and becomes less prone

DOI: 10.13009/EUCASS2023-854

to the separation.

7. Acknowledgments

Authors warmly thank Nunzia Favaloro, the TEDS project manager, who made it possible to conduct the present study.

References

[1] N. Favaloro; G. Saccone; F. Piscitelli; R. Volponi; P. Leoncini; P. Catalano; A. Visingardi; M. C. Noviello. Enabling Technologies for Space Exploration Missions: The CIRA-TEDS Program Roadmap Perspectives. *Aerotecnica Missili & Spazio*, 2023.

[2] Anyoji; Numata; Nagai; Asai. Effects of Mach Number and Specific Heat Ratio on Low-Reynolds-Number Airfoil Flows. *AIAA Journal*, Vol. 53(No. 6), 2015.

[3] F. W. Schmitz. Aerodynamics of the Model Airplane Part1. *NASA, Technical Rept.*, NASA-TM-X-60976, 1967.

[4] Munday; Taira; Suwa; Numata; Asai. Nonlinear Lift on a Triangular Airfoil in Low-Reynolds-Number Compressible Flow. *Journal of Aircraft*, 2015.

[5] Anyoji; Nonomura; Aono; Oyama; Fujii; Nagai; Asai. Computational and Experimental Analysis of a High-Performance Airfoil Under Low-Reynolds-Number Flow Condition. *Journal of Aircraft*, Vol. 51(No. 6), November/December 2014.

[6] Koning; Johnson; Grip. Improved Mars Helicopter Aerodynamic Rotor Model for Comprehensive Analyses. *AIAA JOURNAL*, Vol. 57(No .9), September 2019.

[7] Tsukamoto; Yonemoto; Makizono; Sasaki; Tanaka; Ikeda; Ochi. Variable-Pressure Wind Tunnel Test of Airfoils at Low Reynolds Numbers Designed for Mars Exploration Aircraft. *Trans. JSASS Aerospace Tech. Japan*, Vol. 14(No. 30):pp. 29–34, 2016.

[8] Rinoie; Kamiya. Laminar Separation Bubbles Formed on Airfoils. *Journal of Japan Society of Fluid Mechanics*, (22):15–22, 2003.

[9] T. J. O'Meara, M. M.; Mueller. Laminar Separation Bubble Characteristics on an Airfoil at Low Reynolds Number. *AIAA Journal*, Vol. 25(No. 8):pp. 1033–1041, 1987.

[10] S. M. Mueller, T. J.; Batill. Experimental Studies of Separation on a Two-Dimensional Airfoil at Low Reynolds Number. *AIAA Journal*, Vol. 20(No. 4):pp. 457–463, 1982.

[11] F. W. Schmitz. The Aerodynamics of Small Reynolds number. *NASA TM*, (51), 1980.

[12] Catalano; Amato. An evaluation of RANS turbulence modelling for aerodynamic applications. *Aerospace Science and Technology*, Vol. 7(No. 7):pp. 493–509, 2003.

[13] Marongiu; Catalano; Amato; Iaccarino. U-ZEN: A computational tool solving U-RANS equations for industrial unsteady applications. *34th AIAA FluidDynamics Conference and Exhibit*, 2004.

[14] Capizzano; Catalano; Marongiu; Vitagliano. URANS modelling of turbulent flows controlled by synthetic jets. *35th AIAA FluidDynamics Conference and Exhibit*, 2005.

[15] Catalano; Mele; Tognaccini. On the implementation of a turbulence model for low Reynolds number flows. *Computers and Fluids*, Vol. 109:pp. 67–71, 2015.

[16] Anyoji; Nose; Ida; Numata; Nagai; Asai. Low Reynolds Number Airfoil Testing in a Mars Wind Tunnel. *AIAA Conference paper*, (4627), 2010.

[17] Catalano; Tognaccini. Turbulence modeling for low-Reynolds number flows. *AIAA Journal*, Vol. 48(No. 8):pp. 1673–1685, 2010.

[18] Nose. PSP Measurement of Pressure Distributions on a Cambered Airfoil for Mars Exploration Airplane. *11th Asian Symposium on Visualization*, (Paper ASV11-2011-10), July 2011.

[19] Anyoji. Aerodynamic Characteristics of Ishii Airfoil at Low Reynolds Numbers. *Proceedings of 8th International Conference on Flow Dynamics*, pages pp. 344–345, 2011.